PHYSICAL REVIEW A **87**, 041402(R) (2013)

High-order-harmonic generation by enhanced plasmonic near-fields in metal nanoparticles

T. Shaaran,[1] M. F. Ciappina,[1,2] R. Guichard,[3] J. A. Pérez-Hernández,[4] L. Roso,[4] M. Arnold,[5]
T. Siegel,[5] A. Zaïr,[5] and M. Lewenstein[1,6]

[1]*ICFO-Institut de Ciències Fotòniques, Mediterranean Technology Park, E-08860 Castelldefels (Barcelona), Spain*
[2]*Department of Physics, Auburn University, Auburn, Alabama 36849, USA*
[3]*Laboratoire Chimie-Physique, Matière et Rayonnement, Universitè Pierre et Marie Curie, UMR 7614, F-75231 Paris Cedex 5, France*
[4]*Centro de Làseres Pulsados, Parque Cientìfico, E-37185 Villamayor, Salamanca, Spain*
[5]*Blackett Laboratory Laser Consortium, Department of Physics, Imperial College London, London SW7 2AZ, United Kingdom*
[6]*Institució Catalana de Recerca i Estudis Avançats, Lluis Companys 23, E-08010 Barcelona, Spain*

(Received 11 February 2013; published 11 April 2013)

We present theoretical investigations of high-order-harmonic generation (HHG) resulting from the interaction of noble gases with localized surface plasmons. These plasmonic near-fields are produced when a metal nanoparticle is subject to a few-cycle laser pulse. The enhanced field, which largely depends on the geometrical shape of the metallic nanostructure, has a strong spatial dependency. We demonstrate that the strong nonhomogeneity of this laser field plays an important role in the HHG process and leads to a significant increase of the harmonic-cutoff energy. In order to understand and characterize this feature, we include the functional form of the laser electric field obtained from recent attosecond streaking experiments [F. Süßmann and M. F. Kling, Proc. SPIE **8096**, 80961C (2011)] in the time-dependent Schrödinger equation. By performing classical simulations of the HHG process we show consistency between them and the quantum-mechanical predictions. These allow us to understand the origin of the extended harmonic spectra as a selection of particular trajectory sets. The use of metal nanoparticles is an alternate way of generating coherent XUV light with a laser field whose characteristics can be synthesized locally.

DOI: 10.1103/PhysRevA.87.041402 PACS number(s): 32.80.Rm, 42.65.Ky, 78.67.Bf

When atoms or molecules are exposed to short and intense laser radiation, nonlinear phenomena are triggered as a consequence of this interaction. Among these phenomena, the high-order-harmonic-generation (HHG) process [1,2] has attracted considerable interest since it is one of the most reliable pathways to generate coherent ultraviolet (UV) to extreme ultraviolet (XUV) light. As a result, HHG has proven to be a robust source for the generation of a petahertz attosecond pulse train [3], which can be temporally confined to a single XUV attosecond pulse, now with kilohertz repetition rates [4]. Thanks to its remarkable properties, HHG can also be used to extract temporal and spatial information with both attosecond and subangstrom resolution on the generating system [5], and it represents a considerable tool to scrutinize the atomic world, with its natural temporal and spatial scales [6–11].

The intuitive physical mechanism behind HHG, for a single atom or molecule, has been well established in the so-called three-step model [12–14]: (i) an electronic wave packet is released to the continuum by tunnel ionization through the potential barrier, which is a consequence of the nonperturbative interaction of the single emitter with the laser field, (ii) the emitted electronic wave packet propagates away from its ionic core in the continuum to be finally driven back when the laser electric field changes its sign, and (iii) upon its return, the electronic wave packet may recombine with the core, and the system relaxes the excess kinetic energy acquired by radiating a high-harmonic photon.

In order to experimentally control the HHG features two main types of approaches have been attempted. The first one is based on controlling the HHG process via the manipulation of the laser field characteristics in time and/or space [15]. The second one is based on controlling macroscopic properties of the target samples (i.e., phase matching), leading to very ingenious target geometries [16–18]. However, these approaches rely on detecting the far-field properties of the harmonic yield, which is a result of collectively adding the harmonic radiation of the single emitters. Therefore, it is legitimate to study how a synthesized single emitter could lead to new parameters for HHG control. Metal nanoparticles are a matter of choice since their spatial geometry and the material used can be chosen to confer a spatial transverse nonhomogeneity to the laser field. One of the first demonstrations of such an effect was obtained for surface plasmonic resonances that can locally amplify the laser field [19], and using such resonances, enhancement greater than 20 dB can be achieved [20,21]. Consequently, when a low-intensity femtosecond laser pulse couples to the plasmonic mode of the metal nanoparticle, it initiates a collective oscillation among free electrons within the metal. A location of highly amplified electric field, exceeding the threshold for HHG, is thus created while these free charges redistribute this field around the metal nanostructure, and by injecting noble gases around the nanoparticle, HHG can be produced. Particularly, while using gold bow-tie-shaped nanostructures, it has been demonstrated that the initial modest laser field can be enhanced sufficiently to generate XUV photons, and the radiation generated from the enhanced laser field, localized at each nanostructure, acts as a pointlike source, enabling collimation of this coherent radiation by means of constructive interference [19].

This localization of the enhancement confers to the transverse laser field profile its nonhomogeneity in the region where the electron dynamics is taking place. In addition, the interaction length along the propagation direction of the laser field is restricted to a few nanometers so that no phase conditions need to be considered in order to observe and

calculate the emitted harmonic yield. Consequently, spatially arranged nanostructures open a wide range of possibilities to enhance or shape the spectral and spatial properties of the fundamental laser field and the harmonic field [19]. These two features imply strong modifications in the harmonic spectra which will raise the interest of the strong-field community to utilize, for instance, nanoparticles surrounded by gas atoms or molecules as a new type of target. Recently, there has been extensive theoretical work looking at HHG driven by nonhomogeneous fields [22–28], and consequently, new prospects and deep understanding of the electron dynamics using these particular fields appear to be timely. However, the initial thrill about the utilization of plasmonic fields for HHG in the XUV range was subject to debate by recent findings [29–31]. Fortunately, alternative ways to amplify coherent light using plasmons were explored (e.g., the production of high-energy photoelectrons using plasmonic enhanced near-fields from dielectric nanoparticles [32], metal nanoparticles [33–35], and metal nanotips [36–40]). Further, the question regarding the damage threshold of such nanotargets has been highlighted and indicates that new routes using an initially low intensity laser field need to be considered [41,42].

In this Rapid Communication we investigate how HHG yield can be controlled using enhanced near-fields. These fields are obtained when a metal spherical nanoparticle is illuminated by a few-cycle laser field. The near-fields then generated present a strong spatial dependence that can be accessible experimentally [43]. The plasmonic enhanced near-field in the vicinity of these nanotargets could act as a femtosecond coherent source and drive strong laser-matter processes in the surrounding atomic or molecular gas, e.g., HHG. In addition, the enhancement of the fundamental laser field reaching one or more orders of magnitude, depending on the nanosytem, would allow us to consider low-input laser intensities and to work well below the damage threshold. Summarizing, the physics described in this Rapid Communication requires electric fields which are (i) spatially inhomogeneous on the subwavelength scale and (ii) intense enough to exceed the HHG threshold in noble gases. The first condition can be achieved by various kinds of evanescent fields or fields near surfaces and edges. For the second condition, one possibility of making these fields strong is to use the fields created by laser-induced plasmons near appropriately designed nanostructures, although other systems could exist. Using both quantum-mechanical and classical approaches, we predict that the signature of such synthesized fields is pronounced in the harmonic cutoffs which now extend far beyond the conventional semiclassical limits.

Numerically modeling HHG is based on the assumption that the driven fields are spatially homogeneous in the region where the electron dynamics takes place, i.e., $\mathbf{E}(\mathbf{r},t) = \mathbf{E}(t)$ and $\mathbf{A}(\mathbf{r},t) = \mathbf{A}(t)$ [44,45]. Nonetheless, near-fields generated in the vicinity of metal nanoparticles are not spatially homogeneous, and we address the question of how such nonhomogeneity could be revealed in the HHG. The *conventional* HHG process has been theoretically tackled using different approaches (see, e.g., [46,47]). In this work, we compute the HHG spectra by including the actual functional form of the laser electric field spatial dependence, obtained experimentally [43], in the dimensionally reduced time-dependent Schrödinger equation (TDSE-1D). The TDSE-1D for a model atom can be written as [44]

$$i\frac{\partial\Psi(x,t)}{\partial t} = \mathcal{H}(t)\Psi(x,t) = \left[-\frac{1}{2}\frac{\partial^2}{\partial x^2} + V_a(x) + V_l(x,t)\right]\Psi(x,t), \quad (1)$$

where for the atomic (model) potential $V_a(x)$, we use a soft-core potential, i.e., $V_a(x) = -\frac{1}{\sqrt{x^2+a^2}}$ [48], and $V_l(x,t)$ represents the potential due to the laser electric field.

Certainly, $V_a(x)$ is not suitable for predicting the actual atomic structural information present in the harmonic spectrum, but it is valid for characterizing the HHG cutoff once the ionization potential I_p of a given atom is set. We use $a = 1.62$ to model xenon atoms with $I_p = 12.1299$ eV (0.446 a.u.), and we assume they are in the ground state before we turn on the laser. Xenon atoms present internal transitions that may have had an implication on the plasmonic interaction (similar to scattering Raman enhancement spectroscopy). However, we have not taken these internal transitions into account because they are not resonant with the laser frequency employed. In fact, according to [49], the only transition that has a frequency close to that of the electric laser field we employed (720 nm, i.e., 1.77 eV photon energy) is $6p_{7/2}$-$5d_{9/2}$ at 699 nm, i.e., 1.72 eV. However, the measured lifetime of the level mentioned (6.8 ns, i.e., 0.147 GHz) corresponds to a bandwidth of 6–7 eV; therefore, although this transition is close, it cannot be resonant by one-photon absorption of the driving laser field employed.

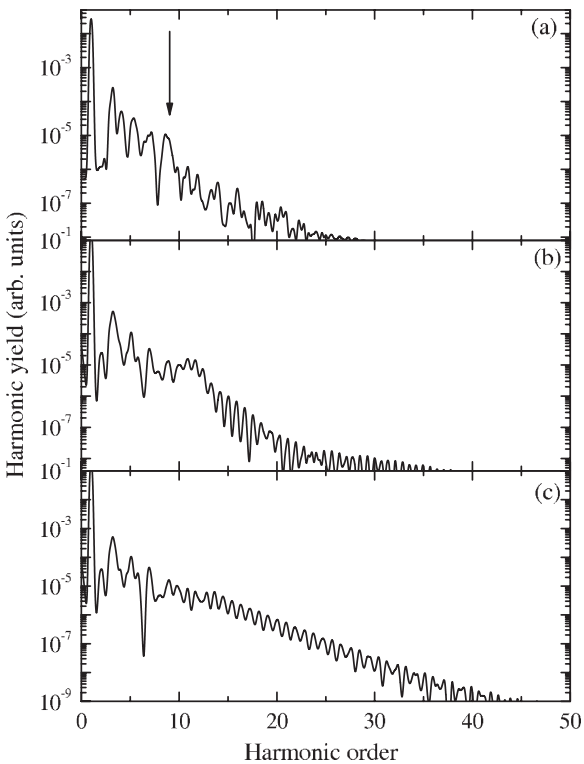

FIG. 1. HHG spectra for Xe, laser wavelength $\lambda = 720$ nm and intensity $I = 2 \times 10^{13}$ W·cm^{-2}. We use a sin^2-shaped pulse with $n = 5$ (see text for details). (a) The homogeneous case, (b) $\chi = 50$, and (c) $\chi = 40$. The arrow in (a) indicates the cutoff predicted by the semiclassical model [13].

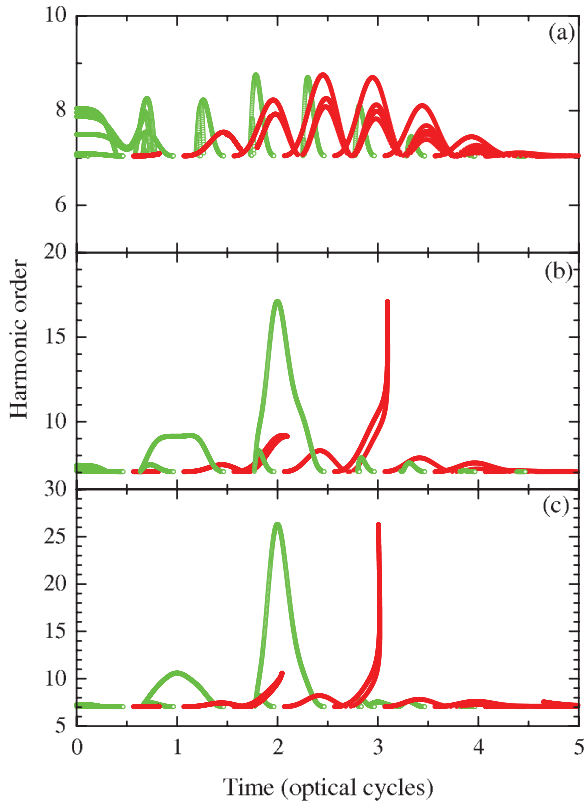

FIG. 2. (Color online) Total energy of the electron (expressed in harmonic order) driven by the laser field calculated from Newton's second law and plotted as a function of t_i [green (light gray) circles] or t_r [red (dark gray) circles]. (a) Homogeneous case, (b) $\chi = 50$, and (c) $\chi = 40$.

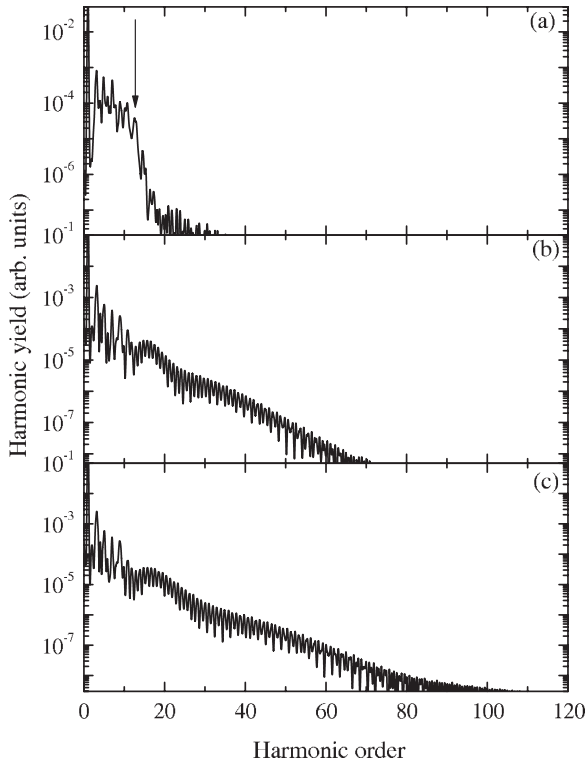

FIG. 3. Same as Fig. 1, but now $I = 5 \times 10^{13}$ W/cm^2.

Equation (1) is solved by using the Crank-Nicolson method [44], and mask functions are used to avoid spurious reflections from the spatial boundaries [50]. $V_l(x,t)$ is given by $V_l(x,t) = -E(x,t)\,x$ and corresponds to a linearly polarized laser electric field in the x axis. We employ the function given by [33] to define $E(x,t)$, i.e., $E(x,t) = E_0\, f(t) \exp(-x/\chi) \sin(\omega t + \phi)$, where E_0, ω, $f(t)$, and ϕ are the peak amplitude, the laser field frequency, the field envelope, and the phase, respectively. The spatial dependence of the plasmonic near-field is given by $\exp(-x/\chi)$, and it depends on the size and the material of the spherical nanoparticle used. $E(x,t)$ is valid for x outside of the metal nanoparticle, i.e., $x \geqslant R_0$, where R_0 is its radius, and it is important to note that the electron motion stands in the region $x \geqslant R_0$, with $(x + R_0) \gg 0$. We consider the laser field with a $\sin^2$ envelope: $f(t) = \sin^2(\frac{\omega t}{2n_p})$, where n_p is the total number of optical cycles, i.e., the total pulse duration is $\tau = 2\pi n_p/\omega$. The harmonic yield of the atom is obtained by Fourier transforming the acceleration $a(t)$ of the electronic wave packet [51].

Figure 1 depicts the harmonic spectra for Xe generated by a laser pulse with $I = 2 \times 10^{13}$ W/cm^2, $\lambda = 720$ nm, and $\tau = 13$ fs, i.e., $n_p = 5$ (this pulse corresponds to an intensity envelope of ≈4.7 fs FWHM) [33]. For the case of a homogeneous field no harmonics beyond the ninth order are observed. The spatial decay constant χ quantifies the nonhomogeneity due to the nanoparticle, and it varies together with its size and the metal employed. Changing χ is therefore equivalent to choosing the type of nanoparticle used, which leads to overcoming the semiclassically predicted cutoff limit and reaching higher harmonic orders. For instance, with $\chi = 40$ and $\chi = 50$, harmonics in the 23rd to 26th order [Fig. 1(c)] and well above the 9th order [a clear cutoff at $n \approx 15$ is visible; Fig. 1(b)], respectively, are observed. A change in the harmonic periodicity, related to breaking the symmetry imposed by the induced nonhomogeneity, is also visible.

We now consider the semiclassical simple man's (SM) model [12,13] in order to characterize the harmonic-cutoff extension. This feature may appear due to the combination of several factors (for details see [24,52]). It is well established that $n_c = (3.17U_p + I_p)/\omega$, where n_c is the harmonic order at the cutoff and U_p is the ponderomotive energy [44]. We solve numerically the Newton equation for an electron moving in an electric field with the same parameters used in the TDSE-1D calculations, i.e., $\ddot{x}(t) = -\nabla_x V_l(x,t) = -E(x,t)(1 - \frac{x(t)}{\chi})$, and consider the SM model initial conditions: the electron starts at position zero at $t = t_i$ (the ionization time) with zero velocity, i.e., $x(t_i) = 0$ and $\dot{x}(t_i) = 0$. When the electric field reverses its direction, the electron returns to its initial position (i.e., the electron *recollides* or recombines with the parent ion) at a later time $t = t_r$ (the recollision time), i.e., $x(t_r) = 0$. The electron kinetic energy at t_r is calculated from $E_k(t_r) = \frac{\dot{x}(t_r)^2}{2}$, and by finding the value of t_r (as a function of t_i) that maximizes E_k, n_c is also maximized.

In Fig. 2 we show the dependence of the harmonic order upon t_i and t_r, calculated from $n = [E_k(t_{i,r}) + I_p]/\omega$ as for the case of Fig. 1. Figures 2(a), 2(b), and 2(c) depict the cases of $\chi \to \infty$ (homogeneous field), $\chi = 50$, and $\chi = 40$, respectively. Figures 2(b) and 2(c) show how the nonhomogeneity of the laser field modifies considerably the

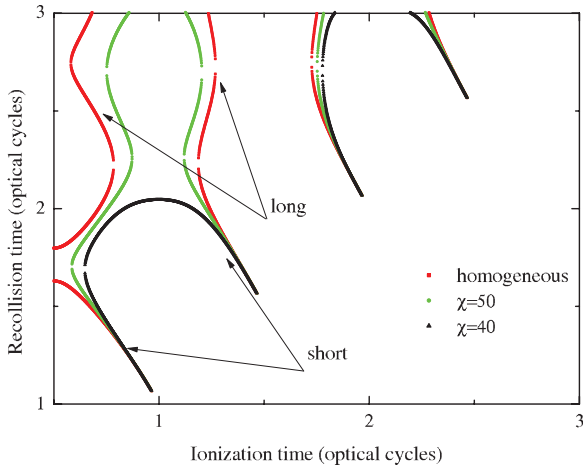

FIG. 4. (Color online) Dependence of the semiclassical trajectories on the ionization (t_i) and recollision (t_r) times for different values of χ. Red (dark gray) squares show the homogeneous case, i.e., $\chi \to \infty$; green (light gray) circles show $\chi = 50$, and black triangles show $\chi = 40$.

electron trajectories towards an extension of n_c. This is clearly present at $n_c \sim 18\omega$ (28 eV) and $n_c \sim 27\omega$ (42 eV) for $\chi = 50$ and $\chi = 40$, respectively. These last two cutoff values are indeed consistent with the quantum-mechanical calculations presented in Fig. 1

Next we compute in Fig. 3 the harmonic spectra by using $I = 5 \times 10^{13}$ W/cm^2, keeping all other parameters the same (we note that the saturation intensity of xenon is $\approx 8 \times 10^{13}$ W/cm^2, and consequently, our proposed values are well below this value). In Figs. 3(b) and 3(c), the nonhomogeneity of the laser field manifests itself as a clear n_c extension, reaching values of $n_c \sim 60\omega$ (93 eV in energy) for $\chi = 40$. These values show a highly nonlinear dependence of n_c on the spatial decay constant χ, and this behavior can be exploited to generate HHG in the XUV regime using modest laser intensities.

Finally, in Fig. 4, we plot t_r of the electron as a function of t_i, as for Fig. 1 (the time is given in optical cycles). For t_i confined between 0.5 and 1.5, the long trajectories are those with $t_r \gtrsim 2.25$, and they are visible only for the homogeneous case [red (dark gray) squares] and for $\chi = 50$ [green (light gray) circles]. On the other hand, short trajectories are characterized by $t_r \lesssim 2.25$, and these are present for both the homogeneous and nonhomogeneous cases. Our results are consistent with those presented in [23,24,52], although in our work we use a different functional form of the electric field resulting from experimental results [33]. We observe how the long trajectories are strongly modified by the nonhomogeneity of the laser field. Indeed the *homogeneous* long trajectories with t_i around 0.75 and 1.25 *converge* with the short one, resulting in a unique trajectory set for $\chi = 40$ (black triangles). Moreover, the branch with $t_i \sim 1.25$ now has t_i smaller than in the homogeneous case; hence the propagation time of the electron in the continuum increases so that it can gain a higher amount of kinetic energy [23,24,26,27,52], as confirmed in the classical calculations presented in Fig. 2. The spatial nonhomogeneity annihilates the long trajectories, and only short trajectories are now responsible for the harmonic spectrum (see [24,25,52,53] for studies using a *linear* nonhomogeneous field)

In conclusion, we present how the HHG from xenon atoms is modified using a plasmonic enhanced near-field generated when a metal nanoparticle is illuminated by a short laser pulse. The functional form of the resulting laser electric field is extracted from attosecond streaking experiments and incorporated in both our quantum and classical-mechanical approaches. We observe in both models an extension of the n_c position that could lead to the production of XUV coherent laser sources and opening the avenue to the generation of attosecond pulses. This feature is a consequence of the induced laser field nonhomogeneity only, which substantially modifies the electron trajectories. A more pronounced increment of the harmonic cutoff, in addition to an appreciable growth in the conversion efficiency, could be reached by varying, for instance, both the radius and the metal material of the spherical nanoparticles. These new degrees of freedom could lead to enhancing the harmonic spectra reaching the XUV regime with modest input laser intensities.

We acknowledge the financial support of the MICINN projects (FIS2008-00784 TOQATA, FIS2008-06368-C02-01, and FIS2010-12834), ERC Advanced Grant QUAGATUA, the Alexander von Humboldt Foundation, and the Hamburg Theory Prize (M.L.). This research has been partially supported by Fundació Privada Cellex. J.A.P.-H. acknowledges support from the Spanish MINECO through the Consolider Program SAUUL (CSD2007-00013) and research project FIS2009-09522, from Junta de Castilla y León through the Program for Groups of Excellence (GR27), and from the ERC Seventh Framework Programme (LASERLAB-EUROPE, Grant No. 228334) A.Z. acknowledges support from EPSRC Grant No. EP/J002348/1 and Royal Society International Exchange Scheme 2012 Grant No. IE120539. L.R. acknowledges the Junta de Castilla y León through the project CLP421A12-1. We thank Matthias Kling and Sergey Zherebstov for useful comments and suggestions.

[1] A. McPherson, G. Gibson, H. Jara, U. Johann, T. S. Luk, I. A. McIntyre, K. Boyer, and C. K. Rhodes, J. Opt. Soc. Am. B **4**, 595 (1987).

[2] A. L'Huillier, K. J. Schafer, and K. C. Kulander, J. Phys. B **24**, 3315 (1991).

[3] P. B. Corkum and F. Krausz, Nat. Phys. **3**, 381 (2007).

[4] A. Scrinzi, T. Westerwalbesloh, U. Kleineberg, U. Heinzmann, M. Drescher, and F. Krausz, Nature (London) **427**, 817 (2004).

[5] M. Lein, J. Phys. B **43**, R135 (2007).

[6] S. Baker, J. S. Robinson, C. A. Haworth, H. Teng, R. A. Smith, C. C. Chirilă, M. Lein, J. G. Tisch, and J. P. Marangos, Science **312**, 424 (2006).

[7] S. Haessler, J. Caillat, W. Boutu, C. Giovanetti-Teixeira, T. Ruchon, T. Auguste, Z. Diveki, P. Breger, A. Maquet, B. Carré *et al.*, Nat. Phys. **6**, 200 (2010).
[8] O. Smirnova, Y. Mairesse, S. Patchkovskii, N. Dudovich, D. Villeneuve, P. Corkum, and M. Y. Ivanov, Proc. Natl. Acad. Sci. USA **106**, 16556 (2009).
[9] O. Smirnova, Y. Mairesse, S. Patchkovskii, N. Dudovich, D. Villeneuve, P. Corkum, and M. Y. Ivanov, Nature (London) **460**, 972 (2009).
[10] Y. Mairesse, A. de Bohan, L. J. Frasinski, H. Merdji, L. C. Dinu, P. Monchicourt, P. Breger, M. Kovačev, R. Taïeb, B. Carré *et al.*, Science **302**, 1540 (2003).
[11] E. P. Power, A. M. March, F. Catoire, E. Sistrun, K. Krushelnick, P. Agostini, and L. F. DiMauro, Nat. Photonics **4**, 352 (2010).
[12] P. B. Corkum, Phys. Rev. Lett. **71**, 1994 (1993).
[13] M. Lewenstein, P. Balcou, M. Y. Ivanov, A. L'Huillier, and P. B. Corkum, Phys. Rev. A **49**, 2117 (1994).
[14] K. J. Schafer, B. Yang, L. F. DiMauro, and K. C. Kulander, Phys. Rev. Lett. **70**, 1599 (1993).
[15] J. A. Pérez-Hernández, M. F. Ciappina, M. Lewenstein, L. Roso, and A. Zaïr, Phys. Rev. Lett. **110**, 053001 (2013).
[16] E. Constant, D. Garzella, P. Breger, E. Mével, C. Dorrer, C. L. Blanc, F. Salin, and P. Agostini, Phys. Rev. Lett. **82**, 1668 (1999).
[17] T. Popmintchev, M. Chen, O. Cohen, M. E. Grisham, J. J. Rocca, M. M. Murnane, and H. C. Kapteyn, Opt. Lett. **33**, 2128 (2008).
[18] T. Popmintchev, M.-C. Chen, A. Bahabad, M. Gerrity, P. Sidorenko, O. Cohen, I. P. Christov, M. M. Murnane, and H. C. Kapteyn, Proc. Natl. Acad. Sci. USA **106**, 10516 (2009).
[19] S. Kim, J. Jin, Y.-J. Kim, I.-Y. Park, Y. Kim, and S.-W. Kim, Nature (London) **453**, 757 (2008).
[20] P. Mühlschlegel, H.-J. Eisler, O. J. F. Martin, B. Hecht, and D. W. Pohl, Science **308**, 1607 (2005).
[21] P. J. Schuck, D. P. Fromm, A. Sundaramurthy, G. S. Kino, and W. E. Moerner, Phys. Rev. Lett. **94**, 017402 (2005).
[22] A. Husakou, S.-J. Im, and J. Herrmann, Phys. Rev. A **83**, 043839 (2011).
[23] I. Yavuz, E. A. Bleda, Z. Altun, and T. Topcu, Phys. Rev. A **85**, 013416 (2012).
[24] M. F. Ciappina, J. Biegert, R. Quidant, and M. Lewenstein, Phys. Rev. A **85**, 033828 (2012).
[25] T. Shaaran, M. F. Ciappina, and M. Lewenstein, Phys. Rev. A **86**, 023408 (2012).
[26] M. F. Ciappina, T. Shaaran, and M. Lewenstein, Ann. Phys. (Berlin, Ger.) **525**, 97 (2013).
[27] B. Fetić, K. Kalajdžić, and D. B. Milošević, Ann. Phys. (Berlin, Ger.) **525**, 107 (2013).
[28] B. Fetić and D. B. Milošević, J. Mod. Opt. (2013), doi: 10.1080/09500340.2013.776122.
[29] M. Sivis, M. Duwe, B. Abel, and C. Ropers, Nature (London) **485**, E1 (2012).
[30] S. Kim, J. Jin, Y.-J. Kim, I.-Y. Park, Y. Kim, and S.-W. Kim, Nature (London) **485**, E2 (2012).
[31] P. B. Corkum (private communication).
[32] S. Zherebtsov *et al.*, Nat. Phys. **7**, 656 (2011).
[33] F. Süßmann and M. F. Kling, Proc. SPIE **8096**, 80961C (2011).
[34] F. Süßmann and M. F. Kling, Phys. Rev. B **84**, 121406(R) (2011).
[35] Y.-Y. Yang, A. Scrinzi, A. Husakou, Q.-G. Li, S. L. Stebbings, F. Süßmann, H.-J. Yu, S. Kim, E. Rühl, J. Herrmann *et al.*, Opt. Express **21**, 2195 (2013).
[36] G. Herink, D. R. Solli, M. Gulde, and C. Ropers, Nature (London) **483**, 190 (2012).
[37] P. Hommelhoff, Y. Sortais, A. Aghajani-Talesh, and M. A. Kasevich, Phys. Rev. Lett. **96**, 077401 (2006).
[38] M. Schenk, M. Krüger, and P. Hommelhoff, Phys. Rev. Lett. **105**, 257601 (2010).
[39] M. Krüger, M. Schenk, and P. Hommelhoff, Nature (London) **475**, 78 (2011).
[40] M. Krüger, M. Schenk, M. Föster, and P. Hommelhoff, J. Phys. B **45**, 074006 (2012).
[41] I.-Y. Park, S. Kim, J. Choi, D.-H. Lee, Y.-J. Kim, M. F. Kling, M. I. Stockman, and S.-W. Kim, Nat. Photonics **4**, 677 (2011).
[42] I.-Y. Park, J. Choi, D.-H. Lee, S. Han, S. Kim, and S.-W. Kim, Ann. Phys. (Berlin, Ger.) **525**, 87 (2013).
[43] M. F. Kling and M. J. J. Vrakking, Annu. Rev. Phys. Chem. **59**, 463 (2008).
[44] M. Protopapas, C. H. Keitel, and P. L. Knight, Rep. Prog. Phys. **60**, 389 (1997).
[45] T. Brabec and F. Krausz, Rev. Mod. Phys. **72**, 545 (2000).
[46] P. Sailères, A. L'Huillier, P. Antoine, and M. Lewenstein, Adv. At. Mol. Phys. **41**, 83 (1999).
[47] A. L'Huillier and M. Lewenstein, in *Strong Field Laser Physics*, edited by T. Brabec, Springer Series in Optical Sciences (Springer, Berlin, 2008), pp. 147–183.
[48] Q. Su and J. H. Eberly, Phys. Rev. A **44**, 5997 (1991).
[49] L. Broström, S. Mannervik, A. Passian, and G. Sundström, Phys. Rev. A **49**, 3333 (1994).
[50] J. L. Krause, K. J. Schafer, and K. C. Kulander, Phys. Rev. A **45**, 4998 (1992).
[51] K. J. Schafer and K. C. Kulander, Phys. Rev. Lett. **78**, 638 (1997).
[52] M. F. Ciappina, S. S. Aćimović, T. Shaaran, J. Biegert, R. Quidant, and M. Lewenstein, Opt. Express **20**, 26261 (2012).
[53] M. F. Ciappina, J. A. Pérez-Hernández, T. Shaaran, J. Biegert, R. Quidant, and M. Lewenstein, Phys. Rev. A **86**, 023413 (2012).